Available online at www.sciencedirect.com
ScienceDirect
Applied Catalysis B: Environmental 78 (2008) 1–10
APPLIED CATALYSIS B: ENVIRONMENTAL
www.elsevier.com/locate/apcatb

# Photocatalytic oxidation of toluene and trichloroethylene in the gas-phase by metallised (Pt, Ag) titanium dioxide

Cissillia Young [a,b], Tuti Mariana Lim [b], Ken Chiang [a], Jason Scott [a,*], Rose Amal [a]

[a] *ARC Centre for Functional Nanomaterials, School of Chemical Sciences and Engineering, The University of New South Wales, Sydney, NSW 2052, Australia*
[b] *Institute of Environmental Science and Engineering, Nanyang Technological University, Innovation Centre, Block 2 Unit 237, 18 Nanyang Drive, Singapore 637723, Singapore*

Received 19 June 2007; received in revised form 13 August 2007; accepted 19 August 2007
Available online 30 August 2007

**Abstract**

The photodegradation of single component and binary mixtures of toluene and trichloroethylene (TCE), on $TiO_2$, $Pt/TiO_2$ and $Ag/TiO_2$ was investigated. Intermediates formed during toluene photodegradation resulted in photocatalyst deactivation. Pt deposits improved the photocatalyst lifetime, delaying toluene breakthrough by up to 2.5 times and improving mineralisation by a factor of 3.5. Ag deposits had a negligible effect on photocatalyst performance. Deactivation was not evident during TCE photodegradation by neat or metallised $TiO_2$. Pt deposits deterred TCE photodegradation with this effect ascribed to poisoning of the metallic Pt sites by photogenerated chloride radicals. In contrast, low Ag loadings were beneficial for TCE photodegradation with this effect ascribed to the temporary interaction between metallic Ag sites and chloride radicals to form AgCl. AgCl possesses semiconductor characteristics which may assist with TCE photodegradation. Photodegradation of the binary toluene/TCE mixture was observed to merge the positive and negative interactions between the metal deposits, organics and intermediates.


*Keywords:* Photocatalysis; Titanium dioxide; Toluene; Trichloroethylene

## 1. Introduction

The presence of atmospheric volatile organic compounds (VOCs) is of concern as they impart adverse effects on human health and the environment. VOCs, such as trichloroethylene (TCE) and toluene are suspected carcinogenic and endocrine disrupting chemicals, respectively. Technologies for removing VOCs include thermal and catalytic oxidation processes, which are energy intensive and, in the case of catalytic oxidation, may be subject to catalyst deactivation by chlorinated VOCs [1]. Photocatalytic oxidation, whereby light is used to activate a semiconductor material, is an alternative technology capable of treating VOCs under ambient conditions, particularly when they are present in low concentrations [2–4].

Titanium dioxide is considered to be an effective photocatalyst as it is chemically and biologically stable, cheap and displays high photoactivity. While $TiO_2$ has shown a capacity for degrading organics, such as 2-propanol [5], methylmercaptan [6] and *n*-decane [7] in the gas-phase, it has also been observed to undergo deactivation by VOCs, such as benzene [8,9], toluene [10–13], *o*-xylene [14], and acetone [15]. Deactivation during toluene photocatalysis has been reported to result from the build-up of carbonaceous species on the $TiO_2$ surface [11,16–18]. Photocatalytic activity can be regenerated using hydrogen peroxide [10], humid air [18] or dry air [11,19,20] under UV illumination; however, irreversible deactivation has been observed after successive regeneration cycles [19].

An established method for improving photocatalyst performance is by depositing noble or platinum group metals, such as Ag or Pt, on the semiconductor surface. The deposits act as electron sinks, favouring separation of the photogenerated charges and enhancing the oxidation and reduction reactions required for organic degradation. However, the role of metal

* Corresponding author at: ARC Centre for Functional Nanomaterials, School of Chemical Sciences and Engineering, The University of New South Wales, Sydney, NSW 2052, Australia. Tel.: +61 2 9385 7966; fax: +61 2 9385 5966.
*E-mail address:* jason.scott@unsw.edu.au (J. Scott).

0926-3373/$ – see front matter 
doi:10.1016/j.apcatb.2007.08.011

deposits in photocatalysis remains controversial as each metal can enhance the degradation of one organic compound yet be detrimental for another [20,21]. For instance, Pt has been shown to improve the photocatalytic degradation of toluene [18,22] but be detrimental for TCE degradation [20,23]. Ag has imparted beneficial effects on the photodegradation of organics containing sulphur [6] while proving detrimental for *n*-butanol [24]. Varying performances of the metal deposits from organic to organic suggest other effects may be evident in conjunction with their role as electron sinks. Surface-adsorbate interactions, the degradation mechanism, and metal deposit properties, such as oxidation state, require consideration to perceive the overall influencing effects [25]. Moreover, the impact heteroatoms in the target organic have on the metal deposits is often overlooked in favour of the intrinsic properties of the metal deposits when attempting to explain observations.

This work contributes to understanding the effect Pt and Ag deposits have on the gas-phase photocatalytic oxidation of toluene and TCE. Single, binary and sequential gas systems of toluene and TCE are considered.

## 2. Experimental

### 2.1. Materials

All experiments used Degussa P25 as the $TiO_2$ source. Quartz wool (5 μm diameter from Saint-Gobain) functioned as the photocatalyst support. Silver (I) nitrate ($AgNO_3$), hexachloroplatinic acid ($H_2PtCl_6$), methanol, sodium chloride (NaCl), nitric acid ($HNO_3$) and hydrochloric acid (HCl) were of analytical grade and used as received. Analytical grade toluene and TCE gases in air were obtained from Linde Gas and National Oxygen (NOX), respectively. Unless otherwise stated, all solutions were prepared using Millipore Milli-Q water with a resistivity of 18.2 MΩcm.

### 2.2. Photocatalyst immobilisation

Impurities were removed from the quartz wool support by washing once with 1% HCl and 10 times with Milli-Q water. Photocatalyst suspensions were prepared by ultrasonically dispersing the photocatalyst in a fixed volume of water for 30 min. An aliquot of this suspension was dripped onto a quartz wool bed packed in a cylindrical quartz photoreactor. The immobilised photocatalyst bed was then dried at 393 K for 5 h.

### 2.3. Pt/$TiO_2$ and Ag/$TiO_2$ preparation

The Pt/$TiO_2$ and Ag/$TiO_2$ particles were prepared by photodeposition. Six hundred millilitres of an ultrasonically treated $TiO_2$ suspension was placed in an annular photoreactor and illuminated (20 W NEC BLB, peak emission 355 nm) for 15 min to remove organic impurities. $H_2PtCl_6$ or $AgNO_3$ precursor solutions were added to the suspension to give the desired metal loading on $TiO_2$. Excess methanol was added as a hole scavenger to assist with complete metal reduction. Prior to photodeposition the suspension pH was adjusted to $3 \pm 0.5$ using $HNO_3$ and purged with 100 mL/min nitrogen for 15 min. Photodeposition was performed for 60 min under a continuous nitrogen purge. The particles were recovered by centrifuging and washed five times with Milli-Q water. They were then dried at 333 K for 24 h and stored in a desiccator. Supernatant, collected during particle recovery, was filtered and analysed using a Perkin-Elmer Optima 2000DV Inductively Coupled Plasma Optical Emission Spectrophotometer (ICP-OES) to ensure complete deposition of the metal precursor on the $TiO_2$ surface. Oxidation states of the Pt and Ag deposits were analysed by X-ray photoelectron spectroscopy (XPS, VG Scientific ESCA LAB 220 i-XL) using Al Kα as the excitation source. Binding energy spectra were recorded in the regions of $C_{1s}$, $Ti_{2p}$, $O_{1s}$, $Pt_{4f}$ and $Ag_{3d}$. To assess the role of chloride ions during photodegradation by Ag/$TiO_2$, a reactor bed comprising 0.66 mmol AgCl supported on washed quartz wool was prepared. This involved washing the quartz wool, packed in a photoreactor, with an $AgNO_3$/NaCl solution and drying at 393 K for 5 h. The dried sample was then washed with MQ water and was re-dried for 5 h at 393 K.

### 2.4. Toluene and TCE photodegradation

Gas-phase photodegradation was performed in a cylindrical quartz photoreactor described elsewhere [22]. In all experiments the quartz photoreactor was illuminated by two 8 W blue–black lamps (Sankyo Denki, $\lambda = 315$–400 nm). Initially, dry air (5 mL/min) was passed through the photoreactor under illuminated conditions to photodegrade adsorbed carbonaceous impurities on the photocatalyst surface. The presence of impurities was assessed by $CO_2$ levels in the reactor effluent with a negligible level of $CO_2$ indicating all impurities had been removed from the photocatalyst surface.

Prior to photodegradation, the target organic was adsorbed on the photocatalyst surface without illumination until saturation was achieved. During photodegradation, relative humidity of the inlet gas stream was maintained at 3% (c.a. 600 ppmv water) and the photoreactor temperature ranged between 298 and 303 K. Toluene ($170 \pm 10$ ppmv) was passed through a photoreactor comprising 50 mg photocatalyst at a flow rate of 6 mL/min. Under non-illuminated conditions the toluene adsorption capacity of Degussa P25 was determined as ($0.74 \pm 0.04$) g toluene/g $TiO_2$. Toluene degradation by AgCl was performed at a toluene concentration of $50 \pm 5$ ppmv and flow rate of 6 mL/min. TCE ($160 \pm 5$ ppmv) was passed through a photoreactor comprising 0.87 mg photocatalyst at a flow rate of 50 mL/min. The TCE conditions were adjusted to provide a more pronounced comparison as TCE was found to be more readily photodegradable than toluene. Under non-illuminated conditions the TCE adsorption capacity of Degussa P25 was determined as ($0.088 \pm 0.005$) g TCE/g $TiO_2$. In binary gas experiments, a mixture of $50 \pm 5$ ppmv toluene and $140 \pm 5$ ppmv TCE, at a flow rate of 6 mL/min, was fed into an illuminated photoreactor containing 50 mg of photocatalyst. To elucidate the effect of chlorinated compounds on photocatalyst performance a sequential run comprising 1 h of $140 \pm 5$ ppmv TCE photodegradation followed by $50 \pm 5$ ppmv toluene

photodegradation was undertaken. Gas flow rate and photocatalyst loading were maintained at 6 mL/min and 50 mg, respectively.

Reactor effluent was automatically sampled (0.5 mL) and monitored by an on-line Agilent 6890N Gas Chromatograph equipped with Flame Ionisation and Thermal Conductivity Detectors (GC/FID/TCD). Dimethylpolysiloxane (Agilent DB-1) and bonded PLOT (Agilent GS-GasPro) columns were used for species separation. The GC was operated isothermally at 306 K, with helium carrier gas flowing at 9.8 mL/min. Detector temperatures were set at 523 K. Unknown peaks obtained by GC/FID were subsequently identified with a GC equipped with a Mass Spectrometer (GC/MS) operating in electron impact (EI) mode.

Organic species deposited on the photocatalyst surface during toluene degradation were extracted by acetonitrile for 24 h. A Waters 2695 High Performance Liquid Chromatograph (HPLC), interfaced with a photodiode array detector (PDA), was used to identify the extracted organics, with an Xterra RP18 column (3.9 mm × 150 mm, 5 μm) and mobile phase comprising a 60:40% water-acetonitrile mixture. X-ray diffraction (Siemens XRD 5000) and XPS (see above) were used to identify inorganic species adsorbed on the photocatalyst surface. XRD analyses were conducted at a scanning rate of 1°/min. To ensure sufficient sample was available to obtain a response during XPS the photocatalyst was pelletised instead of immobilised onto quartz wool and 500 mg packed into the reactor. The photocatalytic degradation profile of the pelletised photocatalyst was verified to be similar to the immobilised photocatalyst.

## 3. Results and discussion

### 3.1. Toluene

Toluene degradation was not evident when illuminated without photocatalyst or passed through the photocatalyst bed without illumination. Figs. 1a and 2a provide toluene concentrations in the reactor effluent following passage through the neat and metallised photocatalyst beds. The profiles can be divided into three stages: (1) an initial rapid decline in the toluene concentration to zero; (2) complete toluene removal for a period of time; and (3) subsequent toluene breakthrough.

Rapid toluene removal during the early reaction stage is likely due to the availability of fresh photocatalyst surface for adsorbing and degrading the toluene. Toluene has been observed by others [13,26] to adsorb on the surface of Degussa P25. During the first stages of photodegradation, toluene undergoes partial oxidation to intermediates, such as benzaldehyde, benzyl alcohol, benzoic acid, benzene, and phenol [10,11,16–18]. The aromatic rings can be ruptured to give aliphatic molecules which can be completely mineralised to $CO_2$. $CO_2$ evolution during toluene photodegradation by the neat and metallised $TiO_2$ is given in Figs. 1b and 2b. The neat

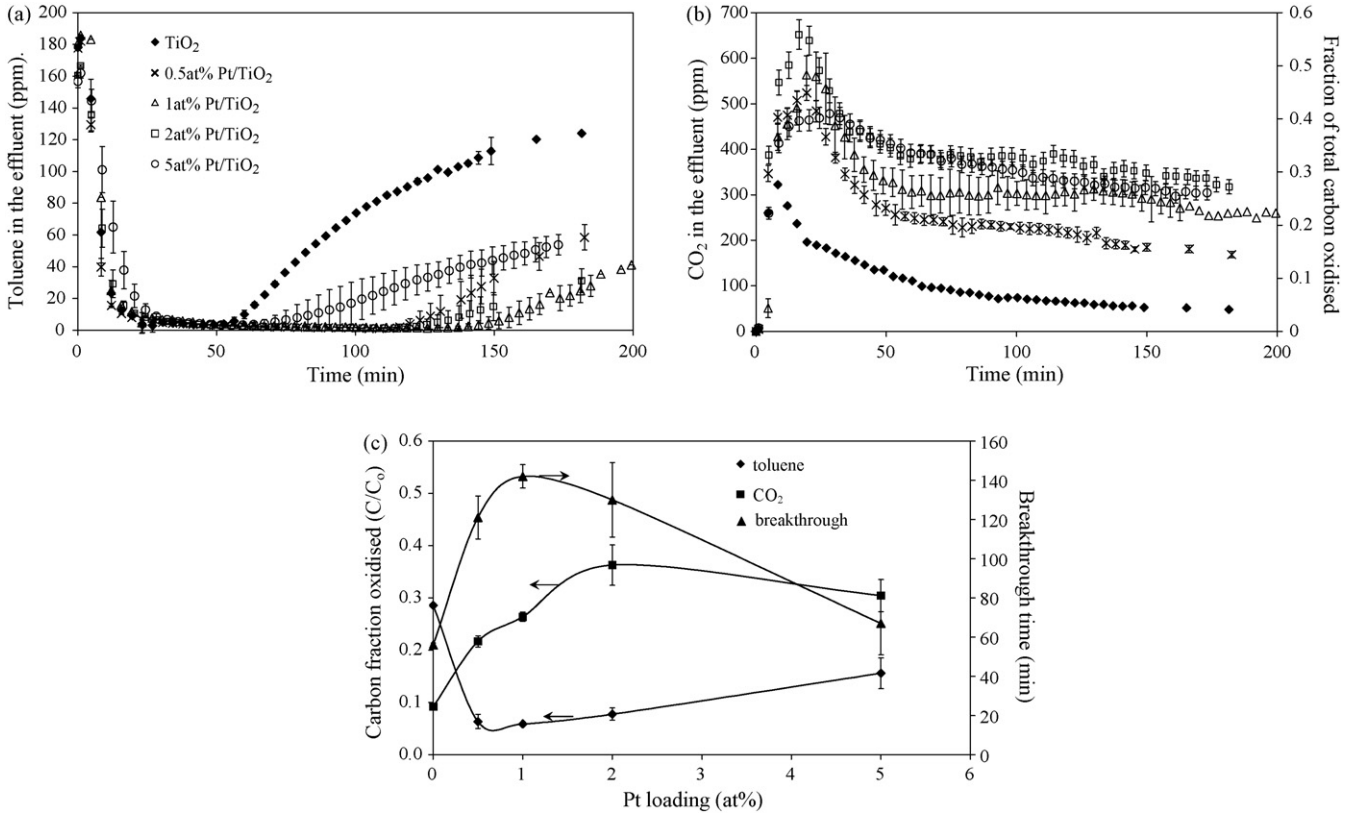


Fig. 1. Photocatalytic profiles of toluene: (a) photodegradation; (b) photomineralisation; and (c) effect of metal loading on breakthrough and fraction of carbon oxidised after 150 min; for Pt photodeposited on Degussa P25. Initial toluene concentration = 170 ± 10 ppmv, make-up gas = air, flow rate = 6 mL/min, photocatalyst loading = 50 mg, Pt loading = 0–5 at%.

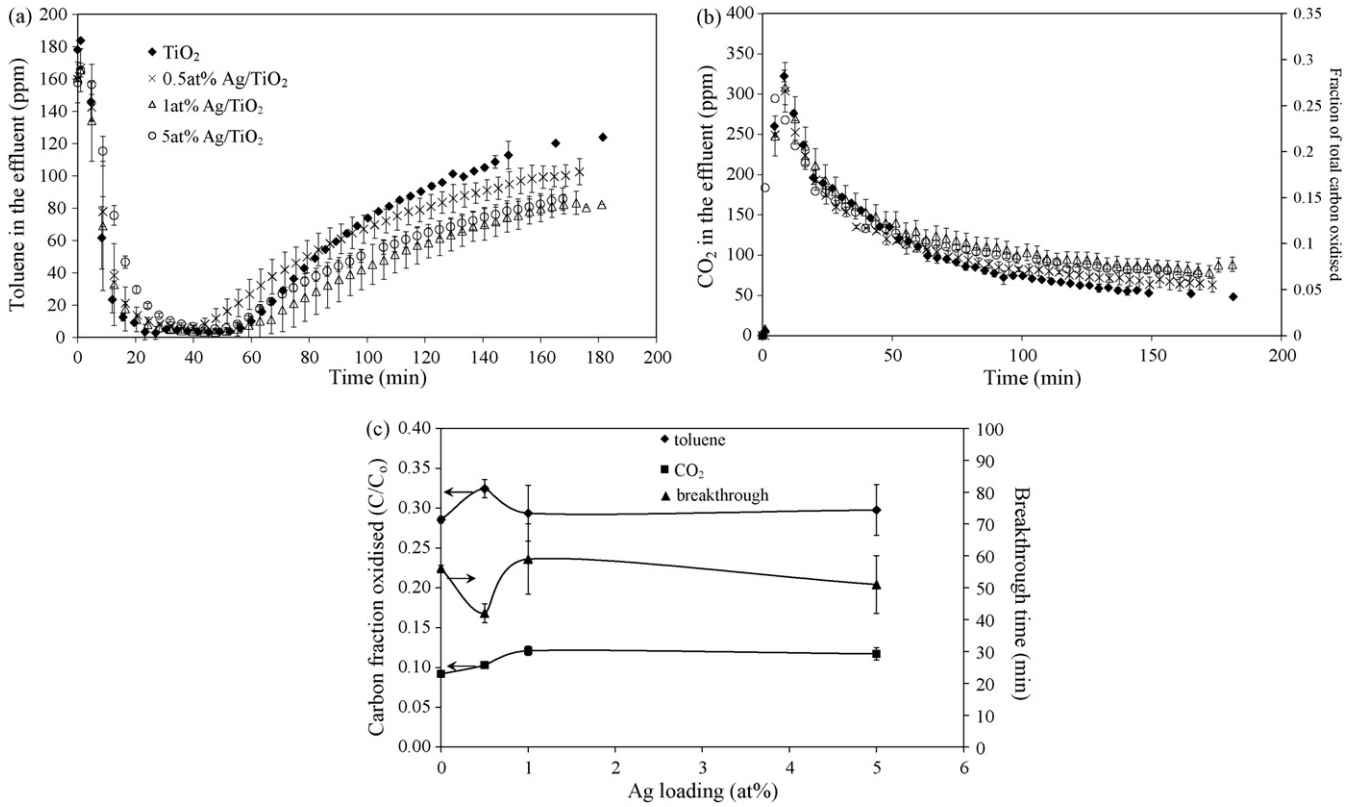


Fig. 2. Photocatalytic profiles of toluene: (a) photodegradation; (b) photomineralisation; and (c) effect of metal loading on breakthrough and fraction of carbon oxidised after 150 min; for Ag photodeposited on Degussa P25. Initial toluene concentration = 170 ± 10 ppmv, make-up gas = air, flow rate = 6 mL/min, photocatalyst loading = 50 mg, Ag loading = 0–5 at%.

$TiO_2$ profile reveals a maximum of 322 ppm $CO_2$ is evolved during photodegradation, corresponding to approximately 27% of the carbon available for oxidation, and indicating incomplete toluene oxidation. This suggests intermediates remain on the $TiO_2$ surface with the subsequent toluene breakthrough indicative of photocatalyst deactivation. Similar findings have been reported by Cao et al. [10], Méndez-Román and Cardona-Martínez [11] and You et al. [27]. HPLC/PDA results in this study detected benzoic acid and several unidentified carbonaceous peaks on the photocatalyst surface, supporting the notion of deactivation by the intermediates.

It is apparent from Fig. 1a and b the presence of Pt deposits on the photocatalyst improve its capacity for degrading toluene and mineralising the intermediates. The effectiveness is a function of Pt loading with the relationship between this and the fractions (as carbon) of unreacted toluene and $CO_2$ generated following 150 min of illumination provided in Fig. 1c. Toluene breakthrough times are included in the figure. The results show a broad optimum Pt loading for toluene removal exists over the range of 0.5–2 at%, when accounting for experimental error. In the context of mineralisation, the optimum Pt loading is 2 at%. Beyond this loading the degree of mineralisation decreases as does the extent of toluene removal.

It is generally accepted improvements by metal deposits on a photocatalyst surface derive from increased electron/hole separation, driven by the need for charge equilibration of the Fermi level across the metal–metal oxide interface [28]. This phenomena increases photogenerated hole availability for oxidation purposes. The metal deposits also facilitate captured electron transfer to reactants and may impart catalytic effects, such as improving $O_2$ dissociation, which can assist in the reduction processes at the metal surface [29,30]. In the case of Pt, oxygen spill over from the Pt deposits to the $TiO_2$ surface has also been reported as a means of improving photocatalysis in the gas-phase [18]. At loadings beyond the optimum it has been suggested the metal deposits can behave as recombination sites due to their obtaining an excessive negative charge which can attract positive holes [25,31]. Additional metal deposits may also shadow the photocatalyst surface from incident light, reducing photocatalyst performance.

The higher degree of mineralisation by the 2 at% $Pt/TiO_2$, despite possessing similar toluene degradation levels as the 0.5 and 1 at% loadings, may derive from this loading being the optimum for degrading a rate-limiting intermediate necessary for mineralisation to proceed. The complexity of the reaction pathway makes identifying such an intermediate difficult. Similar effects regarding optimum metal loadings for parent compound removal and mineralisation have been reported by Dobosz and Sobczyński [32] for the aqueous-phase photodegradation of phenol by $Ag/TiO_2$. They found the optimum Ag loading for phenol removal to be 0.5 wt% but observed the same Ag loading had a negligible effect on phenol mineralisation. While they provided no reason for this discrepancy, Vamathevan et al. [21] attributed the negligible influence of Ag deposits on phenol mineralisation as due to a ‘‘short-circuiting’’ cycle induced by the reversible oxidation of

the phenol intermediate hydroquinone to benzoquinone, negating the increased electron/hole separation.

Fig. 2a and b indicates that the Ag deposits have negligible effect on photocatalyst performance. This is confirmed in Fig. 2c which shows minor variations in toluene reacted and $CO_2$ generated with increasing Ag loading lie within experimental error. The variation in performance of the two metals may be attributed to their respective work functions (Pt = 5.36–5.63 eV, Ag = 4.26–4.29 eV) [34,35] relative to $TiO_2$ (4.6–4.7 eV) [21,33]. The greater positive difference between Pt and $TiO_2$ compared to Ag and $TiO_2$ provides greater electron attraction and trapping resulting in improved electron/hole separation. The marginally lower work function of Ag compared with $TiO_2$ suggests no electron attraction or trapping will occur, giving little improvement in photocatalytic performance.

The XPS spectra of the fresh Pt/$TiO_2$ and Ag/$TiO_2$, given in Fig. 3a and b, respectively, show a higher proportion of Ag atoms are in an oxidised state compared with Pt. The percentage of each metal possessing a particular oxidation state was estimated by the areas of the corresponding XPS peaks. These values are provided in Table 1 and indicate approximately 17% of the Pt is in the +2 oxidation state while approximately 53% of the Ag is in the +1 oxidation state. The remaining percentage comprises the metallic state of each metal. The differences in the proportion of oxidised metal

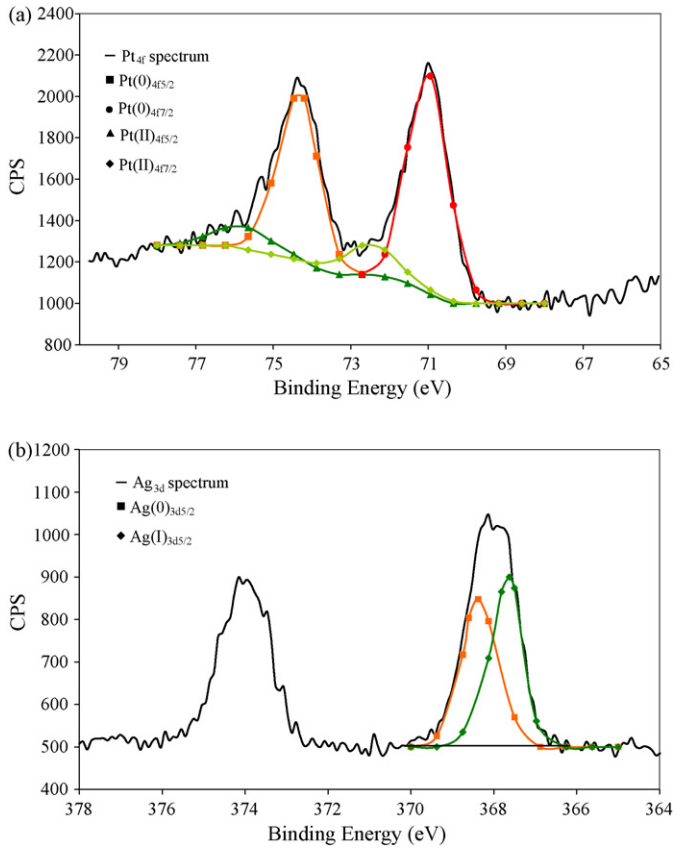


Fig. 3. XPS spectra of: (a) fresh 1 at% $Pt_{4f}/TiO_2$ photocatalyst; (b) fresh 1 at% $Ag_{3d}/TiO_2$ photocatalyst. Spectra include deconvolution peaks identifying Pt(0), Pt(II) and Ag(0), Ag(I), respectively.

Table 1
Percentages of metallic and oxidised Pt and Ag in metals photodeposited on the surface of Degussa P25

| | Fresh | | Used (TCE) | |
|---|---|---|---|---|
| | Pt (%) | Ag (%) | Pt (%) | Ag (%) |
| Oxidised | 17 | 53 | 58 | 100 |
| Metal | 83 | 47 | 42 | 0 |

Values provided for fresh metallised $TiO_2$ and metallised $TiO_2$ following photodegradation of TCE alone, a mixture of TCE and toluene, and TCE photodegradation followed by toluene photodegradation. Metal loading = 1 at%.

formed during photodeposition may be explained by the higher redox potential of Pt compared with Ag, as given in Eqs. (1) and (2) below:

$$Pt^{2+} + 2e^- \leftrightarrow Pt^0 \qquad E^0 = 1.18\,V \tag{1}$$

$$Ag^+ + e^- \leftrightarrow Ag^0 \qquad E^0 = 0.80\,V \tag{2}$$

The higher redox value for Pt indicates its greater affinity for electrons whereby it is more readily reduced. Photoreduced metals have also been observed to undergo reoxidation on exposure to air [36] which may also be a contributing factor.

Several researchers have reported the oxidation state of noble metal deposits on the $TiO_2$ surface may affect photocatalyst performance [25,37,38]. Sano et al. reported similar oxidation state distributions for Pt and Ag photodeposited on Degussa P25 [39], suggesting they can influence photocatalytic performance. They found oxidised Pt provided a reduced improvement compared with metallic Pt for the gas-phase photodegradation of acetaldehyde. They ascribed the benefit invoked by metallic Pt over oxidised Pt to its ability to generate active oxygen species ($O_2^{\bullet}$). In contrast, the photoactivity of oxidised Ag was greater than metallic Ag, but lower than neat Degussa P25, for the same reaction. Sano et al. reported $O_2^{\bullet}$ generation not to be important for Ag in this case with other factors, such as alternate active species or Ag dispersion to be more influential.

### 3.2. TCE

No TCE degradation was evident when illuminated without photocatalyst or when exposed to the photocatalyst without illumination. Figs. 4 and 5 display the gas-phase photodegradation profiles for TCE by Pt/$TiO_2$ and Ag/$TiO_2$, respectively. The system typically reached steady-state TCE conversion and $CO_2$ generation within 30 min of illumination with no observed photocatalyst deactivation or intermediates detected in the effluent over a 24 h reaction period. These findings indicate TCE is more readily photodegraded by $TiO_2$ than toluene with this being attributed [40,41] to the generation of chlorine radicals (Eqs. (3) and (4)). The chlorine radicals trigger chain reactions, which assist in degrading TCE and its intermediates on the surface and in the bulk phase [9,23,42–48] as shown in Eqs. (5)–(10).

$$TiO_2 + h\nu \rightarrow e^- + h^+ \tag{3}$$

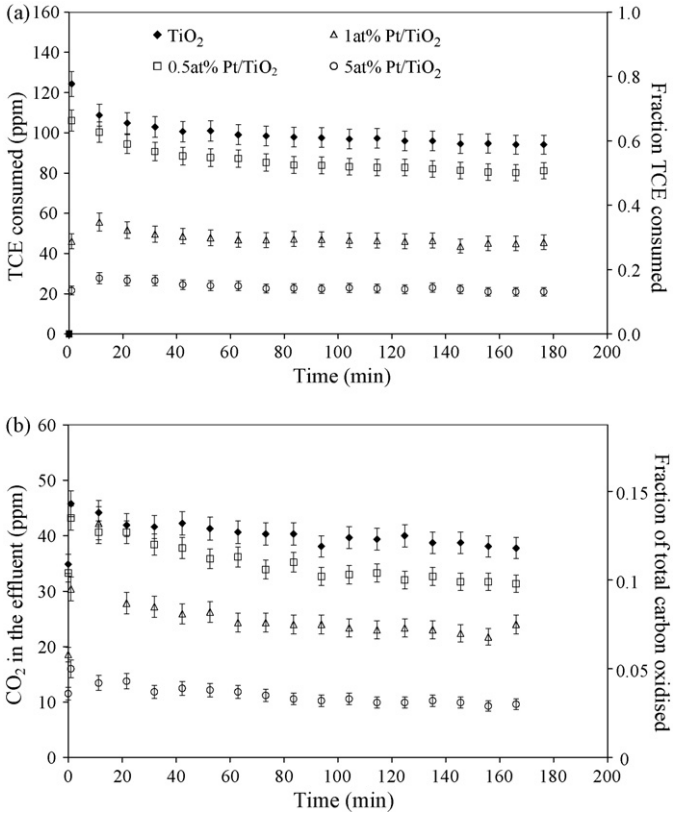


Fig. 4. Pt loading effect on TCE: (a) photodegradation; (b) photomineralisation by Degussa P25. Initial TCE concentration = 160 ± 5 ppmv, make-up gas = air, flow rate = 50 mL/min, photocatalyst loading = 0.87 mg.

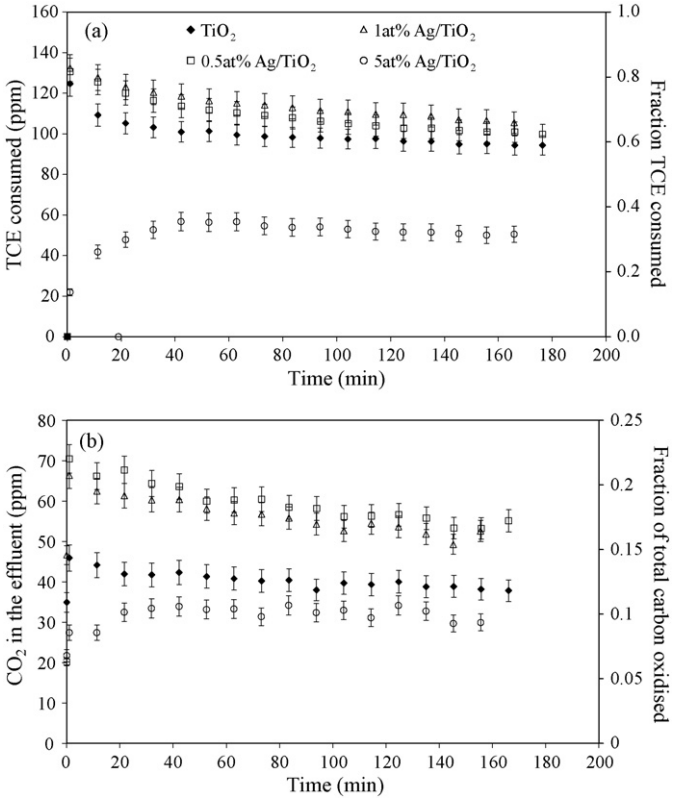


Fig. 5. Ag loading effect on TCE: (a) photodegradation; (b) photomineralisation by Degussa P25. Initial TCE concentration = 160 ± 5 ppmv, make-up gas = air, flow rate = 50 mL/min, photocatalyst loading = 0.87 mg.

$$h^+ + Cl^- \rightarrow Cl^\bullet \quad (4)$$

$$CClHCCl_2 + Cl^\bullet \rightarrow C^\bullet ClHCCl_3 \quad (5)$$

$$CClHCCl_2 + Cl^\bullet \rightarrow CCl_2HC^\bullet Cl_2 \quad (6)$$

$$CCl_2HC^\bullet Cl_2 + O_2 \rightarrow CCl_2HCCl_2OO^\bullet \quad (7)$$

$$2CCl_2HCCl_2O_2^\bullet \rightarrow 2CCl_2HCCl_2O^\bullet + O_2 \quad (8)$$

$$CCl_2HCCl_2O^\bullet \rightarrow CCl_2(O) + CHCl_2 \quad (9)$$

$$CCl_2HCCl_2O^\bullet \rightarrow CCl_2HCCl(O) + Cl^\bullet \quad (10)$$

The effect of Pt on the photodegradation and mineralisation of TCE is shown in Fig. 4a and b. The enhancement invoked by Pt during toluene photodegradation is not observed for TCE, with the Pt deposits reducing TCE consumption and mineralisation. As the Pt loading increases, the extent of TCE degradation decreases (Fig. 6). Sano et al. [49] observed Pd photodeposits on Degussa P25 decreased the gas-phase photodegradation of vinyl chloride monomer while Driessen and Grassian [23] observed 0.1–2% Pt deposits on Degussa P25 to be detrimental for TCE photodegradation. Both cited the metal deposits blocking the most active sites ($Ti^{3+}$) as the main reason for the negative effect. However, the benefits seen for Pt deposits on toluene photodegradation infer this is not the case as photoactive site blockage would generally be expected as detrimental for all organics. This implies an alternate effect is the source of the observed negative influence which is discussed later. The behaviour of the Ag deposits during TCE photodegradation differed from the Pt deposits as illustrated in Fig. 5a and b. Ag loadings of 0.5 and 1 at% improved TCE photodegradation and mineralisation while a loading of 5 at% decreased photocatalyst performance (Fig. 6).

XPS spectra of the chlorine ($Cl_{2p1/2}$, $Cl_{2p3/2}$) peaks on used $Pt/TiO_2$ and $Ag/TiO_2$ photocatalysts are given in Fig. 7a and b, respectively. Organic and inorganic chlorine were detected on

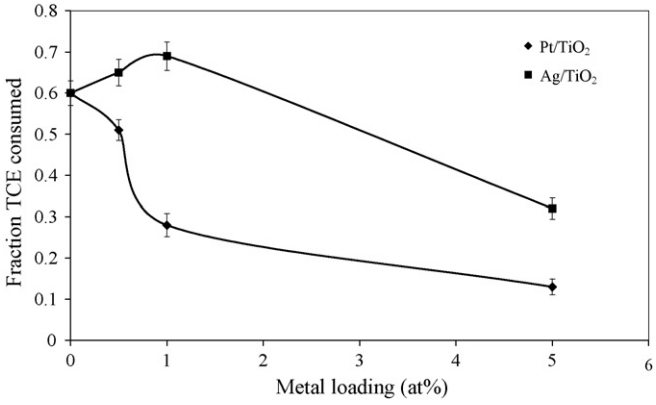


Fig. 6. Pt and Ag loading effect on steady-state photocatalytic TCE consumption. Initial TCE concentration = 160 ± 5 ppmv, flow rate = 50 mL/min, photocatalyst loading = 0.87 mg.

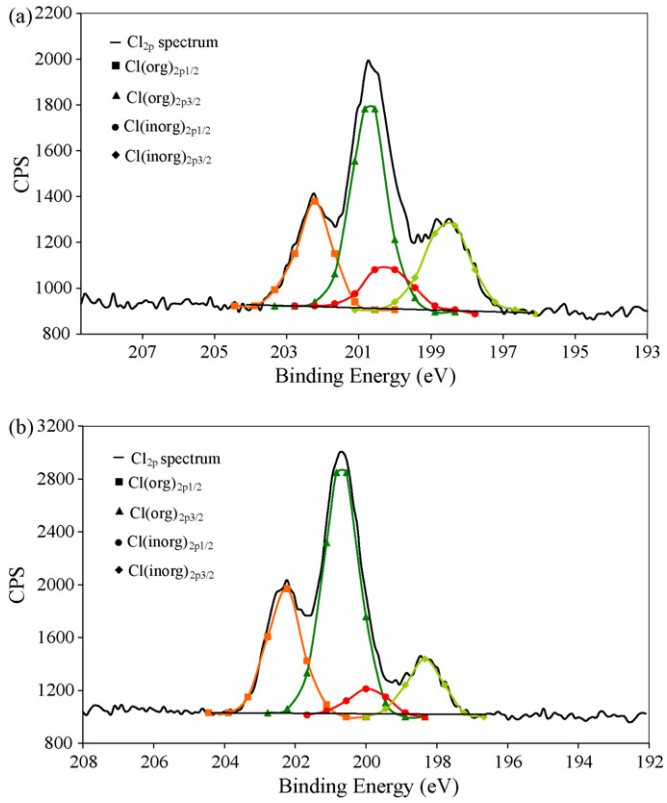


Fig. 7. Chlorine$_{2p}$ XPS spectra of: (a) 1 at% Pt/$TiO_2$; and (b) 1 at% Ag/$TiO_2$ photocatalysts following TCE photodegradation. Spectra include deconvolution peaks ($Cl_{2p1}$, $Cl_{2p3}$) identifying organic and inorganic chlorine.

both used photocatalysts. The Cl peak at c.a. 200.7 eV represents organic chlorine while the peak at c.a. 198.3 eV represents inorganic chlorine [50]. The XPS spectra show the used Pt/$TiO_2$ particles possess a higher ratio of inorganic to organic chlorine on the surface than the Ag/$TiO_2$ particles, with the percentage of each component given in Table 2. The organic chlorine on the used photocatalyst likely results from surface-adsorbed TCE or chlorinated intermediates while the inorganic chlorine peak may be due to Cl interaction with Ti and/or the metal deposits. Comparing the XPS Pt peaks ($Pt_{4f5/2}$, $Pt_{4f7/2}$) before and after TCE photodegradation (Table 3) shows a positive shift of ~0.3 eV for the peaks corresponding to Pt(0) while there is a positive shift of ~0.7 eV for the peaks corresponding to Pt(II). This shift in peak binding energy implies interaction between the Pt deposits and the Cl from TCE. Zhang and Beard [51] observed a positive binding energy shift of 0.7 eV for $Pt_{4d5/2}$ peaks following treatment of Pt/$Al_2O_3$ with $NH_4Cl$. They suggested this shift derived from the formation of $Pt_nCl_x$ on the alumina surface.

Table 2
Normalised atomic percentages of organic and inorganic chlorine on neat and 1 at% metallised (Pt, Ag) $TiO_2$ following TCE and sequential TCE and toluene photodegradation

| Used photocatalyst | | Organic $Cl_{2p}$ | Inorganic $Cl_{2p}$ |
|---|---|---|---|
| Following TCE oxidation | Pt/$TiO_2$ | 2.30 | 1.25 |
| | Ag/$TiO_2$ | 3.72 | 0.91 |
| Following sequential TCE and toluene oxidation | $TiO_2$ | 0.00 | 0.00 |
| | Pt/$TiO_2$ | 0.31 | 0.32 |
| | Ag/$TiO_2$ | 0.00 | 0.00 |

Table 3
$Pt_{4f5/2}$ and $Pt_{4f7/2}$ XPS peak binding energies for Pt(0) and Pt(II) prior to and following TCE photodegradation

| | Binding energy (eV) | | | |
|---|---|---|---|---|
| Peak | $Pt(0)_{4f5/2}$ | $Pt(0)_{4f7/2}$ | $Pt(II)_{4f5/2}$ | $Pt(II)_{4f7/2}$ |
| Fresh Pt/$TiO_2$ | 74.2 | 70.8 | 75.5 | 72.2 |
| Used (TCE) Pt/$TiO_2$ | 74.5 | 71.1 | 76.2 | 72.9 |
| Shift | 0.3 | 0.3 | 0.7 | 0.7 |

Included is the extent of shift in binding energies resulting from TCE photodegradation.

The XPS analysis indicated the percentage of oxidised Pt increased from 17 to 58% during TCE photodegradation (Table 1), which is anticipated to derive from oxidation of the Pt deposits by the Cl radicals (Table 2). Pt oxidation may contribute to the decrease in photoactivity in accordance with the discussion of Sano et al. [39]. Other contributing factors deriving from the interaction between Pt and Cl may include:

1. a decrease in chlorine availability for generating chlorine radicals. These radicals are critical for enhancing TCE degradation (Eqs. (5)–(10));
2. impeding the role of Pt metal in electron transfer. The chlorine radicals can compete for photogenerated electrons at the Pt surface (Eq. (11)), reducing generation of other active species (e.g. $O_2^{\bullet -}$).

$$Cl^{\bullet} + e^{-} \rightarrow Cl^{-} \quad (11)$$

   The resulting chloride ion reacts to form PtCl which has not been reported in the literature to possess photocatalytic properties or facilitate electron transfer;
3. blocking possible catalytic properties of the Pt deposits. In selected cases [52] Pt deposits have been shown to possess thermal catalytic oxidative properties under ambient conditions which may assist, in particular, in oxidising the intermediates. Cl is known to be detrimental to Pt catalysis [53] and has been observed to cause complete deactivation of Pt metals [54].

The XPS analysis indicated the Ag deposits were completely oxidised during TCE photodegradation (Table 1). Comparing this finding with the TCE photodegradation results for Ag (Fig. 6) indicates any beneficial influence Ag oxidation imparts on photocatalytic performance of the deposits is limited as doubling the level of oxidised Ag deposits does not give a corresponding increase in TCE consumption. XPS spectra indicated a positive shift from 367.6 to 367.8 eV in the $Ag(I)_{3d5/2}$ peak binding energy for fresh and used Ag/$TiO_2$ suggesting Cl interacts with the Ag deposits. In this instance, the interaction between Ag deposits and Cl radicals (Table 2) to form AgCl, may benefit the photocatalyst, particularly at lower Ag loadings. The positive effects of chlorine on Ag in the form of AgCl photocatalysts has also been observed by others [55–57]. The use of AgCl

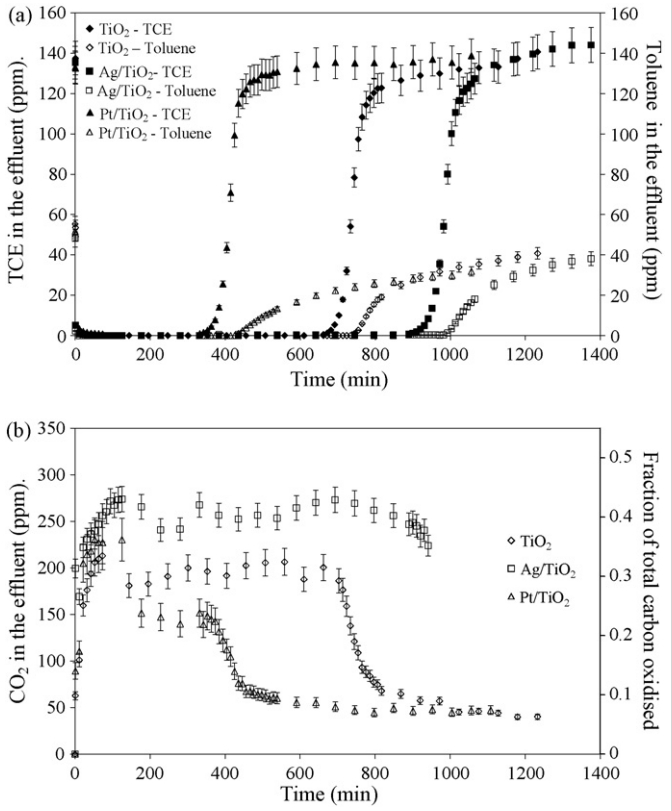


Fig. 8. Effect of Pt and Ag deposits on photooxidation of binary toluene/TCE system: (a) toluene and TCE photodegradation profiles; (b) toluene and TCE photomineralisation profiles. Initial toluene = 50 ppmv, initial TCE concentration = 140 ppmv, make-up gas = air, flow rate = 6 mL/min, photocatalyst loading = 50 mg, $TiO_2$ support = Degussa P25, metal loading = 1 at%.

(band gap energy = 3.3 eV corresponding to a 380 nm onset wavelength) as a photocatalyst for water oxidation has been reported by Currao et al. [56,57]. In some instances chlorine has been intentionally added to Pd or Ag catalysts to enhance the partial oxidation of hydrocarbons [58].

### 3.3. Toluene and TCE

The photodegradation results for the binary toluene and TCE mixture by $TiO_2$, $Pt/TiO_2$ and $Ag/TiO_2$ are shown in Fig. 8. In this system both TCE and toluene breakthrough are evident. TCE breakthrough indicates the intermediates formed during toluene degradation again act to deactivate the photocatalyst surface. Coincidental with TCE breakthrough is a rapid decrease in $CO_2$ concentration in the reactor effluent with the difference providing an estimate of the degree of TCE mineralisation at this point. The values are provided in Table 4 and illustrate the suppression of TCE conversion invoked by toluene. The concentration of $CO_2$ remaining in the effluent, following removal of the TCE component, indicates approximately 13% of the carbon in toluene is being mineralised. Luo and Ollis [19] have similarly reported the quenching of TCE conversion in the presence of toluene. Table 5 compares breakthrough times for neat and metallised $TiO_2$ in the binary system and shows TCE breakthrough occurs prior to toluene for each photocatalyst. This implies TCE is more weakly

Table 4
Fraction of available TCE oxidised (as $CO_2$) at breakthrough point for neat and 1 at% metallised (Pt, Ag) $TiO_2$ during photodegradation of binary toluene/TCE mixture

| Photocatalyst | Fraction TCE oxidised (as $CO_2$) |
|---|---|
| $TiO_2$ | 0.55 |
| $Pt/TiO_2$ | 0.36 |
| $Ag/TiO_2$ | 0.78 |

Toluene inlet concentration = 50 ppmv, TCE inlet concentration = 140 ppmv, flow rate = 6 mL/min, catalyst loading = 50 mg.

Table 5
Toluene and TCE breakthrough times for neat and 1 at% metallised (Pt, Ag) $TiO_2$ during photodegradation in single and binary systems

| | Single system (h)[a] | | | Binary system (h)[a] | | |
|---|---|---|---|---|---|---|
| | $TiO_2$ | $Pt/TiO_2$ | $Ag/TiO_2$ | $TiO_2$ | $Pt/TiO_2$ | $Ag/TiO_2$ |
| Toluene | 6.5 | 13.4 | 8 | 10.5 | 7.3 | 17 |
| TCE | No breakthrough observed | | | 9.5 | 5.5 | 15 |

Toluene inlet concentration = 50 ppmv, TCE inlet concentration = 140 ppmv, flow rate = 6 mL/min, catalyst loading = 50 mg.
[a] Variation in breakthrough times estimated as ±1.5 h.

adsorbed on the photocatalyst surface than toluene and its intermediates.

The comparison between breakthrough times for the single component and binary systems (Table 5) shows toluene removal was enhanced by the presence of TCE during photocatalysis by neat $TiO_2$. Luo and Ollis [19] reported toluene photodegradation to be enhanced in a mixed toluene/TCE reactant stream. Furthermore, d'Hennezel and Ollis [50] demonstrated $TiO_2$ surface pre-chlorination by HCl enhanced the photocatalytic degradation efficiency of toluene and hexane. They concluded surface chlorine atoms were converted to chlorine radicals which reacted with the toluene and assisted in its oxidation to $CO_2$. In the present study, enhanced toluene degradation in the binary mixture may be explained by the presence of chlorine radicals generated from the photodegradation of TCE. They promote degradation of the toluene and its intermediates and delay toluene breakthrough.

Fig. 8a shows Pt deposits are detrimental for photodegrading toluene and TCE in the binary system compared to neat $TiO_2$. $CO_2$ generation prior to breakthrough is also markedly reduced (Fig. 8b). The negative effect likely results from the same factors described previously for the TCE system and may be further amplified by the poisoning effect of chlorine on Pt favouring the formation of oligomer or carbon-containing residue [59]. It is apparent the consequences of the interaction between Pt and Cl are detrimental not only for TCE photodegradation but for other organics which coexist in the gas stream.

Conversely, Ag deposits prolong photocatalyst lifetime and enhance the extent of mineralisation in the binary system compared with neat $TiO_2$. As the Ag deposits imparted no significant effects during toluene photodegradation, the enhancement shown in the binary system is likely due to the presence of TCE. That is, the generated chloride radicals react with the Ag deposits to form photocatalytically active AgCl.

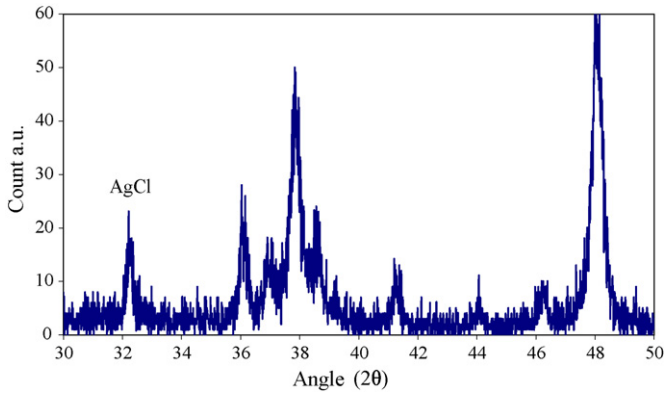


Fig. 9. XRD spectra of $Ag/TiO_2$ following photodegradation of TCE. Illustrates presence of AgCl on the $TiO_2$ surface.

The interaction between chlorine radicals from the TCE and Ag deposits was confirmed by XRD with Fig. 9 indicating the presence of AgCl on the spent $Ag/TiO_2$ photocatalyst following the binary gas reaction process. Moreover, AgCl was found to remove toluene only under illuminated conditions (Fig. 10) with GC–MS positively identifying three chlorinated species (1-chloro-2-methylbenzene; 1-chloro-3-methylbenzene; 1,3-dichloro-2-methylbenzene) in the reactor effluent. No $CO_2$ was detected indicating the AgCl was unable to completely mineralise the toluene. These findings support the notion of AgCl playing a role in the toluene photooxidation. Upon illumination, a charge transfer from $Cl^-$ to $Ag^+$ is initiated producing Cl radicals [56,57] (Eq. (12)). The chlorine radicals may participate in toluene degradation (Eq. (13)) or recombine to form chlorine which subsequently reacts with toluene (Eq. (14)). The electron remaining with the Ag atom may react with species, such as molecular oxygen to form superoxide radicals which participate in the oxidation process (Eq. (15)).

$$(Ag^+)(Cl^-) + h\nu \rightarrow Ag^\bullet + Cl^\bullet \quad (12)$$

$$Cl^\bullet + C_7H_8 \rightarrow \text{chlorinated intermediates} \quad (13)$$

$$Cl^\bullet + Cl^\bullet \rightarrow Cl_2 + C_7H_8 \rightarrow \text{chlorinated intermediates} \quad (14)$$

$$Ag^\bullet + O_2 \rightarrow O_2{}^\bullet + \text{toluene} \rightarrow \text{oxidised intermediates} \quad (15)$$

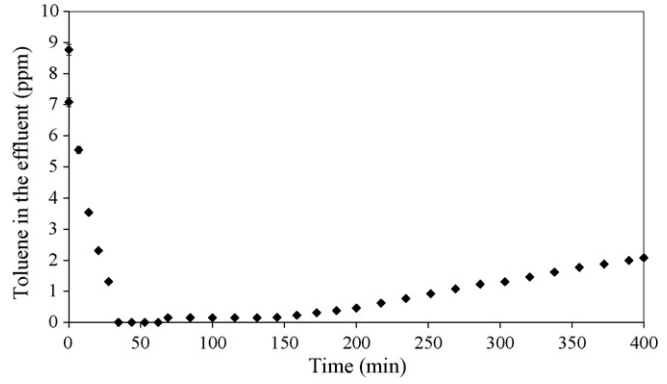


Fig. 10. Toluene photodegradation profile by AgCl. Initial toluene concentration = 50 ± 5 ppmv, make-up gas = air, flow rate = 6 mL/min, AgCl loading = 0.66 mmol.

XPS analyses on spent photocatalysts, following consecutive photocatalytic runs involving TCE and toluene (Table 2), revealed no $Cl_{2p}$ signals were present for the neat $TiO_2$ and $Ag/TiO_2$ particles, while Cl signals were detected for the $Pt/TiO_2$ photocatalyst. This indicates Cl species on the bare $TiO_2$ and $Ag/TiO_2$ are consumed during toluene photodegradation and highlights a non-permanent interaction between Ag and Cl under illumination. Moreover, it supports the proposed mechanism involving chlorine detachment via photo-excited electron transfer from $Cl^-$ to $Ag^+$. In contrast, the Cl peaks remaining on the spent $Pt/TiO_2$ indicate the interaction between Pt and Cl on $Pt/TiO_2$ is more stable.

## 4. Conclusions

Gas-phase photodegradation of toluene deactivated Degussa P25 through the build-up of intermediates on the photocatalyst surface. Pt deposits improved photocatalyst performance by prolonging photocatalyst life, while Ag deposits had a minimal effect. Photocatalyst deactivation did not occur during the photodegradation of TCE. Pt deposits were detrimental to photocatalyst activity while low loadings of Ag deposits were mildly beneficial. XPS data indicated the proportion of oxidised Pt and Ag increased during TCE photodegradation and detected inorganic chlorine on the spent photocatalyst surface. This implies chlorine radicals, generated during TCE photodegradation, interact with the metal deposits to:

1. produce PtCl which negates the positive effects typically invoked by Pt deposits by hindering their electron capturing and transferring capabilities during photocatalysis;
2. produce AgCl which is a known semiconductor and may be beneficial for the photocatalytic process in this case through temporarily trapping Cl radicals.

Photodegrading a binary mixture of toluene and TCE merged the impacts of the organics and the metal deposits on the photocatalytic process. Chlorine radicals from TCE delayed toluene breakthrough whereas photogenerated toluene intermediates deactivated the photocatalyst surface resulting in TCE breakthrough. Pt deposits were detrimental when photodegrading the binary mixture, suspected to be due to the negative interaction between Pt and Cl radicals. Ag deposits improved photodegradation of the binary mixture due to the positive interaction between Ag and Cl radicals. The findings of this study show positive and negative photocatalytic effects imparted by metal deposits can be strongly influenced by the nature of the organic and its intermediates as well as by interactions between the metal deposits and photogenerated species.

## Acknowledgements

The authors would like to thank Dr. Bill Gong, School of Chemistry, The University of New South Wales, for his assistance with the XPS analyses and The Institute of Environmental Science and Engineering, Nanyang Technological University, for funding C. Young's scholarship.

## References


[1] J. Corella, J.M. Toledo, A.M. Padilla, Appl. Catal. B: Environ. 27 (2000) 243–256.
[2] S.B. Kim, S.C. Hong, Appl. Catal. B: Environ. 35 (2002) 305–315.
[3] S.A. Larson, J.L. Falconer, Catal. Lett. 44 (1997) 57–65.
[4] D.S. Muggli, S.A. Keyser, J.L. Falconer, Catal. Lett. 55 (1998) 129–132.
[5] C. Colmenares, M.A. Aramendía, A. Marinas, F.J. Urbano, Appl. Catal. A: Gen. 306 (2006) 120–127.
[6] S. Kato, Y. Hirano, M. Iwata, T. Sano, K. Takeuchi, S. Matsuzawa, Appl. Catal. B: Environ. 57 (2005) 109–115.
[7] R. Nakamura, S. Sato, J. Phys. Chem. B 106 (2002) 5893–5896.
[8] H. Einaga, S. Futamura, T. Ibusuki, Appl. Catal. B: Environ. 38 (2002) 215–225.
[9] X. Fu, W.A. Zeltner, M.A. Anderson, Appl. Catal. B: Environ. 6 (1995) 209–224.
[10] L. Cao, Z. Gao, S.L. Suib, T.N. Obee, S.O. Hay, J.D. Freihaut, J. Catal. 196 (2000) 253–261.
[11] R. Méndez-Román, N. Cardona-Martínez, Catal. Today 40 (1998) 353–365.
[12] C. Belver, M.J. López-Muñoz, J.M. Cornado, J. Soria, Appl. Catal. B: Environ. 46 (2003) 497–509.
[13] R.M. Alberici, W.F. Jardim, Appl. Catal. B: Environ. 14 (1997) 55–68.
[14] M.M. Ameen, G.B. Raupp, J. Catal. 184 (1999) 112–122.
[15] L. Zhang, J.C. Yu, Catal. Commun. 6 (2005) 684–687.
[16] V. Augugliaro, S. Coluccia, V. Loddo, L. Marchese, G. Martra, L. Palmisano, M. Schiavello, Appl. Catal. B: Environ. 20 (1999) 15–27.
[17] M.C. Blount, J.L. Falconer, J. Catal. 200 (2001) 21–33.
[18] M.C. Blount, J.L. Falconer, Appl. Catal. B: Environ. 39 (2002) 39–50.
[19] Y. Luo, D.F. Ollis, J. Catal. 163 (1996) 1–11.
[20] A. Linsebigler, C. Rusu, J.T. Yates Jr., J. Am. Chem. Soc. 118 (1996) 5284–5289.
[21] V. Vamathevan, R. Amal, D. Beydoun, G. Low, S. McEvoy, Chem. Eng. J. 98 (2004) 127–139.
[22] C. Young, T.M. Lim, K. Chiang, R. Amal, Water Sci. Technol. 50 (2004) 251–256.
[23] M.D. Driessen, V.H. Grassian, J. Phys. Chem. B 102 (1998) 1418–1423.
[24] Y. Chapuis, D. Klvana, C. Guy, J. Kirchnerova, J. Air Waste Manage. Assoc. 52 (2002) 845–854.
[25] J. Lee, W. Choi, J. Phys. Chem. B 109 (2005) 7399–7406.
[26] A. Bouzaza, C. Vallet, A. Laplanche, J. Photochem. Photobiol. A: Chem. 177 (2006) 212–217.
[27] Y.S. You, K.H. Chung, Y.M. Kim, J.H. Kim, G. Seo, Korean J. Chem. Eng. 21 (2003) 58–64.
[28] R. Dalven, Introduction to Applied Solid State Physics, second ed., Plenum Press, New York and London, 1990.
[29] Z. Yang, J. Li, X. Yang, X. Xie, Y. Wu, J. Mol. Catal. A: Chem. 241 (2005) 15–22.
[30] H. Einaga, A. Ogata, S. Futamura, T. Ibusuki, Chem. Phys. Lett. 38 (2001) 303–307.
[31] J.C. Yang, Y.C. Kim, Y.G. Shul, C.H. Shin, T.K. Lee, Appl. Surf. Sci. 121–122 (1997) 525–529.
[32] A. Dobosz, A. Sobczyński, Water Res. 37 (2003) 1489–1496.
[33] I.M. Arabatzis, T. Stergiopoulos, D. Andreeva, S. Kitova, S.G. Neophytides, P. Falaras, J. Catal. 220 (2003) 127–135.
[34] J. Hölzl, F.K. Schulte, Springer Tracts Mod. Phys. 85 (1979) 1–150.
[35] J.C. Rivière, Solid State Surface Science, vol. 1, Marcel Dekker, New York, 1969.
[36] T.H. Fleisch, G.W. Zajac, J.O. Schreiner, G.J. Mains, Appl. Surf. Sci. 26 (1986) 488–497.
[37] I. Ait-Ichou, M. Formenti, S.J. Teichner, Stud. Surf. Sci. Catal. 17 (1983) 63–75.
[38] J.-M. Herrmann, P. Pichat, Stud. Surf. Sci. Catal. 17 (1983) 77–87.
[39] T. Sano, N. Negishi, K. Uchino, J. Tanaka, S. Matsuzawa, K. Takeuchi, J. Photochem. Photobiol. A: Chem. 160 (2003) 93–98.
[40] S. Ozaki, L. Zhao, T. Amemiya, K. Itoh, M. Murabayashi, Appl. Catal. B: Environ. 52 (2004) 81–89.
[41] H.-H. Ou, S.-L. Lo, J. Hazard. Mater. 146 (2007) 302–308.
[42] C.H. Hung, B.J. Marinas, Environ. Sci. Technol. 31 (1997) 562–568.
[43] G. Huybrechts, G. Martens, L. Meyers, J. Olbregts, K. Thomas, Trans. Faraday Soc. 61 (1965) 1921–1932.
[44] G. Huybrechts, J. Olbregts, K. Thomas, Trans. Faraday Soc. 63 (1967) 1647–1655.
[45] G. Huybrechts, L. Meyers, Trans. Faraday Soc. 62 (1966) 2191–2199.
[46] E. Berman, J. Dong, in: W.W. Eckenfelder, A.R. Bowen, J.A. Roth (Eds.), Proceedings of the Third International Symposium on Chemical Oxidation: Technology for the Nineties, Technomic Publishers, Chicago, 1993, pp. 183–189.
[47] L. Bertrand, J.A. Franklin, P. Goldfinger, G. Huybrechts, J. Phys. Chem. 72 (1968) 3926–3928.
[48] M.L. Sauer, M.A. Hale, D.F. Ollis, J. Photochem. Photobiol. A: Chem. 88 (1995) 169–178.
[49] T. Sano, S. Kutsuna, N. Negishi, K. Takeuchi, J. Mol. Catal. A: Chem. 189 (2002) 263–270.
[50] O. d'Hennezel, D.F. Ollis, Helv. Chim. Acta 84 (2001) 3511–3518.
[51] Z.C. Zhang, B.C. Beard, Appl. Catal. A: Gen. 188 (1999) 229–240.
[52] F. Denny, J. Scott, K. Chiang, W.Y. Teoh, R. Amal, J. Mol. Catal. A: Chem. 263 (2007) 93–102.
[53] V.I. Kovalchuk, J.L. d'Itri, Appl. Catal. A: Gen. 271 (2004) 13–25.
[54] J.M. Toledo, J. Corella, A. Sanz, Environ. Prog. 20 (2001) 167–174.
[55] K. Pfanner, N. Gfeller, G. Calzaferri, J. Photochem. Photobiol. A: Chem. 95 (1996) 175–180.
[56] A. Currao, V.R. Reddy, G. Calzaferri, ChemPhysChem 5 (2004) 720–724.
[57] A. Currao, V.R. Reddy, M.K. van Veen, R.E.I. Schropp, G. Calzaferri, Photochem. Photobiol. Sci. 3 (2004) 1017–1025.
[58] M. Moonsiri, P. Rangsunvigit, S. Chavadej, E. Gulari, Chem. Eng. J. 97 (2004) 241–248.
[59] M. Thomassen, B. Børresen, G. Hagen, R. Tunold, Electrochim. Acta 50 (2005) 1157–1167.